A Hybrid Aluminium Alloy and its Zoo of Interacting Nano-Precipitates

Sigurd Wenner[1], Calin Daniel Marioara[2], Sigmund Jarle Andersen[2], Martin Ervik[1] and Randi Holmestad[1]*

[1]Department of Physics, NTNU, Høgskoleringen 5, NO-7491 Trondheim, Norway
[2]Materials and Chemistry, SINTEF, Høgskoleringen 5, NO-7491 Trondheim, Norway
*Phone: +47 73594197 Fax: +47 73591410 E-mail: sigurd.wenner@ntnu.no

Abstract

An alloy with aluminium as its base element is heat treated to form a multitude of precipitate phases known from different classes of industrial alloys: Al–Cu(–Mg), Al–Mg–Si–Cu, and Al–Zn–Mg. Nanometer-sized needle-shaped particles define the starting point of the phase nucleation, after which there is a split in the precipitation sequence into six phases of highly diverse compositions and morphologies. There are several unique effects of phases from different alloy systems being present in the same host lattice, of which we concentrate on two: the replacement of Ag by Zn on the Ω interface and the formation of combined plates of the θ' and C phases. Using atomically resolved scanning transmission electron microscopy and energy-dispersive X-ray spectroscopy, we investigate the formation mechanisms, crystal structures and compositions of the precipitates.

Keywords: aluminium alloys, nucleation, phase transformations, transmission electron microscopy

1. Introduction

Optimizing the properties of metallic alloys requires control over crystalline phases: their volume fraction in the material, their extent and shape, and the structure and strain around phase boundaries. A classic, and very important example of phase transformation is diffusion-controlled nucleation and growth from a solid solution in a host lattice. A phase nucleates

when a sufficient amount of solute elements has converged on a location, after which it grows into its most energetically favorable shape. In addition to age hardenable Al alloys, examples of alloy systems exhibiting this mechanism are various Fe alloys [1,2], Cu–Co [3], Cu–Ni–Si [4], Mg–Y/Gd [5,6], and even doped non-metallic compounds such as the ferroelectric $BiFeO_3$–Nd–Ti [7]. There typically exists a precipitation sequence, where a phase with a lower bulk enthalpy nucleates in connection to another precipitate in the host lattice. In many cases, the sequence is branched, so that several different phases can precipitate at a given time in the microstructural evolution.

Focusing on alloys with fcc-Al as their host, the three main classes of wrought heat-treatable alloys are, in their most basic forms, Al–Cu (2*xxx*), Al–Mg–Si (6*xxx*), and Al–Zn–Mg (7*xxx*). For improvement of mechanical strength, they all rely on nanometer-sized precipitate phases, which are partially coherent with the host lattice. The Al–Cu system is the oldest, predating the discovery that nano-precipitates are responsible for strengthening during heat treatment [8,9]. Cu is often supplemented by Mg, Ag, and/or Li to improve properties, resulting in precipitate phases of diverse geometries and orientations [10,11]. The Al–Mg–Si system has the densest precipitation of the three classes, despite being relatively low-solute. This is mainly attributed to Si, which has a low solubility in Al and provides a driving force for homogeneous nucleation [12,13], which is why it is often added to all types of Al alloys in small amounts. In Al–Mg–Si–Cu, the most important strengthening phases are β'' needles [14], Q' needles [15, 16] and C plates [17]. The Al–Zn–Mg system is hardened by precipitation of the precursors to the equilibrium η–Zn_2Mg phase. These early phases come in several variants, some of which lack a repeated unit cell [18, 19, 20].

For decades, precipitates in aluminium alloys have been studied extensively with transmission electron microscopy (TEM). A specimen used for TEM has a thickness of roughly 50 nm,

which means that a nanometer-sized plate- or needle-shaped precipitate embedded in a host lattice can be imaged in cross-section (as a 2D projection) without any overlap with other phases in the viewing direction. High-angle annular dark-field scanning TEM (HAADF–STEM) has become a common technique for imaging nano-precipitates. This applies especially to cases where elements with a high difference in atomic number (e.g. Al and Cu) are present, as HAADF–STEM produces readily interpretable images with high atomic number-contrast [21]. Already in the 1970s, this technique was used to image single heavy atoms such as Au and Pt on carbon films [22,23]. The technique is at its most useful in an aberration-corrected microscope. Assuming the existence of high symmetry orientations having projected atom–atom distances longer than ~0.1 nm, every atomic column in a lattice may be imaged. Upon combination with a spectroscopy technique such as electron energy loss spectroscopy (EELS) [24] or energy-dispersive X-ray spectroscopy (EDS) [25], compositional mapping with atomic resolution becomes feasible for a suitably thin and stable specimen.

The accumulated knowledge from both early X-ray diffraction and later TEM imaging/diffraction experiments should enable us to predict which precipitate phases are present in any industrial Al alloy with a specific heat treatment. In this paper, we transcend the boundaries between the previously mentioned systems by investigating an alloy with a composition that accommodates the important strengthening phases in all three systems. The goal is to observe any interactions between the very different phases that may form, and to better understand how some phases heterogeneously nucleate on existing precipitates. Knowledge on precipitation in hybrid alloys has a great significance in industry as recycled material of varying composition constitute a growing portion of all aluminium production. The main analytical tools are atomic-resolution HAADF–STEM imaging and simultaneous EDS acquisition with near-atomic resolution. In the Results and Discussion section, we start

by presenting all phases appearing during over-aging of the alloy. A discussion on nucleation follows, after which we focus on the two precipitate phases Ω and θ', and how their interfaces with the host lattice are modified by introducing elements outside their "native" alloy systems into the material.

2. Experimental Procedure

An alloy with the nominal composition Al–4.0% Zn–2.0% Cu–1.0% Mg–0.70% Si–0.55% Mn–0.20% Fe (by weight) was cast as a 4 kg billet. Mn and Fe were added to create Al(Mn,Fe)Si [26]/$Al_{20}Cu_2Mn_3$ [11,27] dispersoid phases which restrict grain growth, and are not present in any of the phases analyzed in the paper. The billet was homogenized at 480 °C for 3 hours, which solutionizes all Zn, Cu and Mg. Some ≈20 μm large Si particles were left undissolved. The billet was extruded to a cylindrical profile with 20 mm cross-sectional diameter. Samples of the profile were kept for 1 hour at 480 °C followed by water quenching and immediate immersion in an oil furnace at 150 °C for up to 32 days. The hardness values were measured with a Struers Duramin-A2500 using a 5 kg force. TEM specimens were prepared by mechanical polishing to 100 μm foils and subsequent electropolishing using a Struers TenuPol-5. The applied voltage was 20 V and the electrolyte was 1/3 nitric acid and 2/3 methanol kept at −25 °C.

HAADF–STEM was done primarily on a double Cs-corrected Jeol ARM-200F cold FEG microscope equipped with a JEOL Centurio EDS detector. A 200 kV, ≈21 pA electron beam with a convergence semi-angle of 27 mrad was used, and the collection semi-angles of the HAADF detector was 42–178 mrad. Some images are slightly distorted due to specimen drift during acquisition. No image processing was applied. For EDS mapping, a beam with ≈200 pA and convergence semi-angle 34 mrad was used to increase the signal, and drift correction was used. EDS maps were created from the integral of the K shell peaks from the relevant

elements. Some lower magnification bright-field TEM, HAADF–STEM and EDS work was done on a Philips CM30 and a Jeol JEM-2100F equipped with an Oxford Aztec EDS system.

3. Results and Discussion

3.1. Microstructure and Phases

Fig. 1(a,c,d) shows the precipitate microstructure at peak hardness (142 HV), which is achieved by keeping our alloy at 150 °C for 17 hours. The precipitates are needle-shaped and oriented along $<001>_{Al}$, with cross-sections reminiscent of small disordered structures previously found in Al–Mg–Si–Cu alloys [28]. The EDS map in Fig. 1(e–j) reveals that all the elements Zn, Cu, Mg and Si are present in the needles. No other types of nano-precipitates were observed at peak hardness. Parts of the disordered needles host a projected hexagonal Si network [29], which seems to create a stable environment for nucleating phases with a wide range of compositions. Some samples were over-aged at 150 °C for up to 32 days [Fig. 1(b)), inducing a hardness decrease to 99 HV. At this point, a substantial selection of phases is present in the material, all shown in Fig. 2. All phases were checked structurally through imaging and compositionally with EDS for identification. As the figure shows only one example of each of the observed phases, we further provide a discussion about their average characteristics relative to reports from the literature.

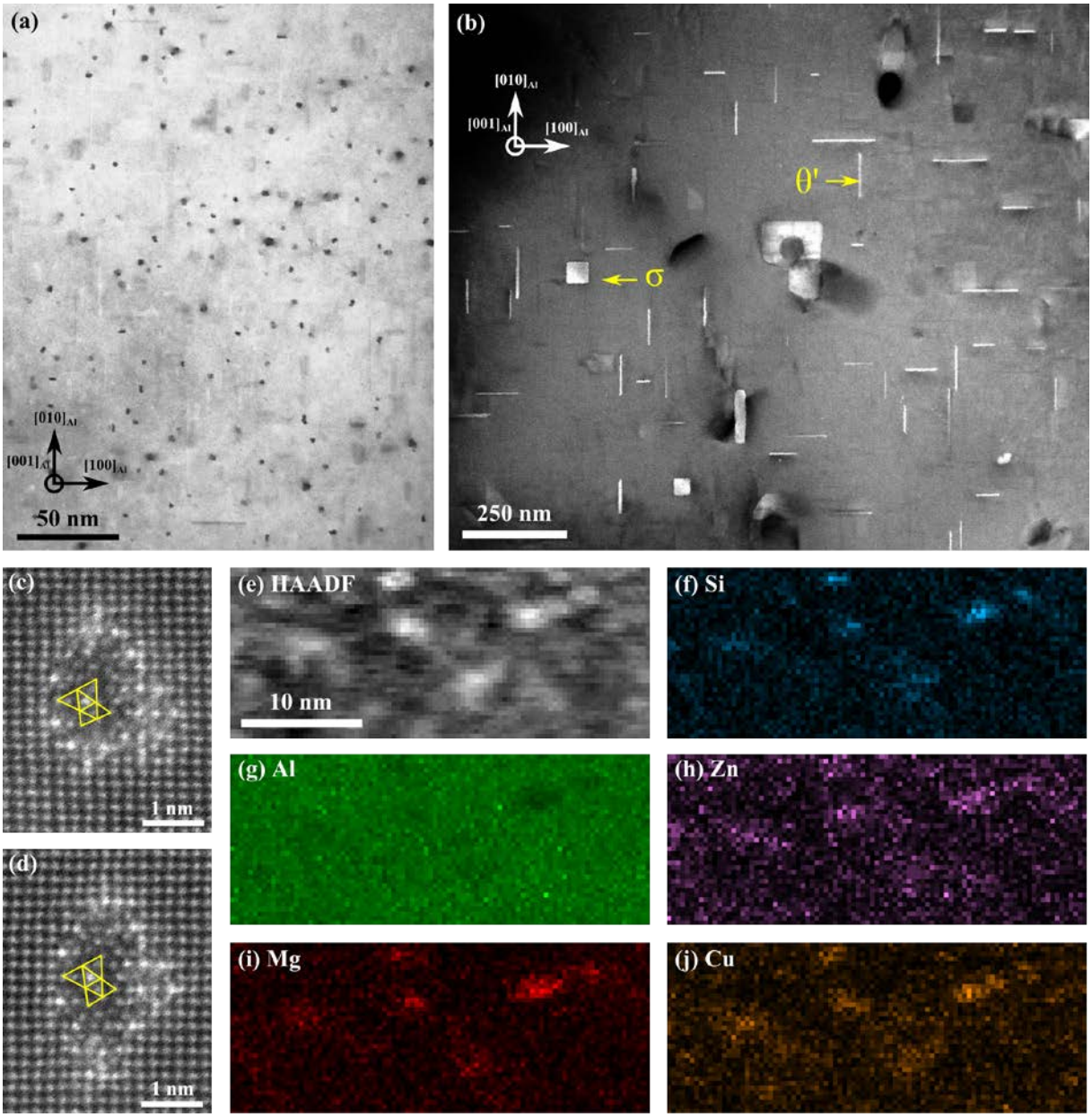
(a)
[010]Al
[001]Al
[100]Al
50 nm
(b)
[010]Al
[001]Al
[100]Al
θ'
σ
250 nm
(c)
1 nm
(d)
1 nm
(e) HAADF
10 nm
(f) Si
(g) Al
(h) Zn
(i) Mg
(j) Cu

Fig. 1.

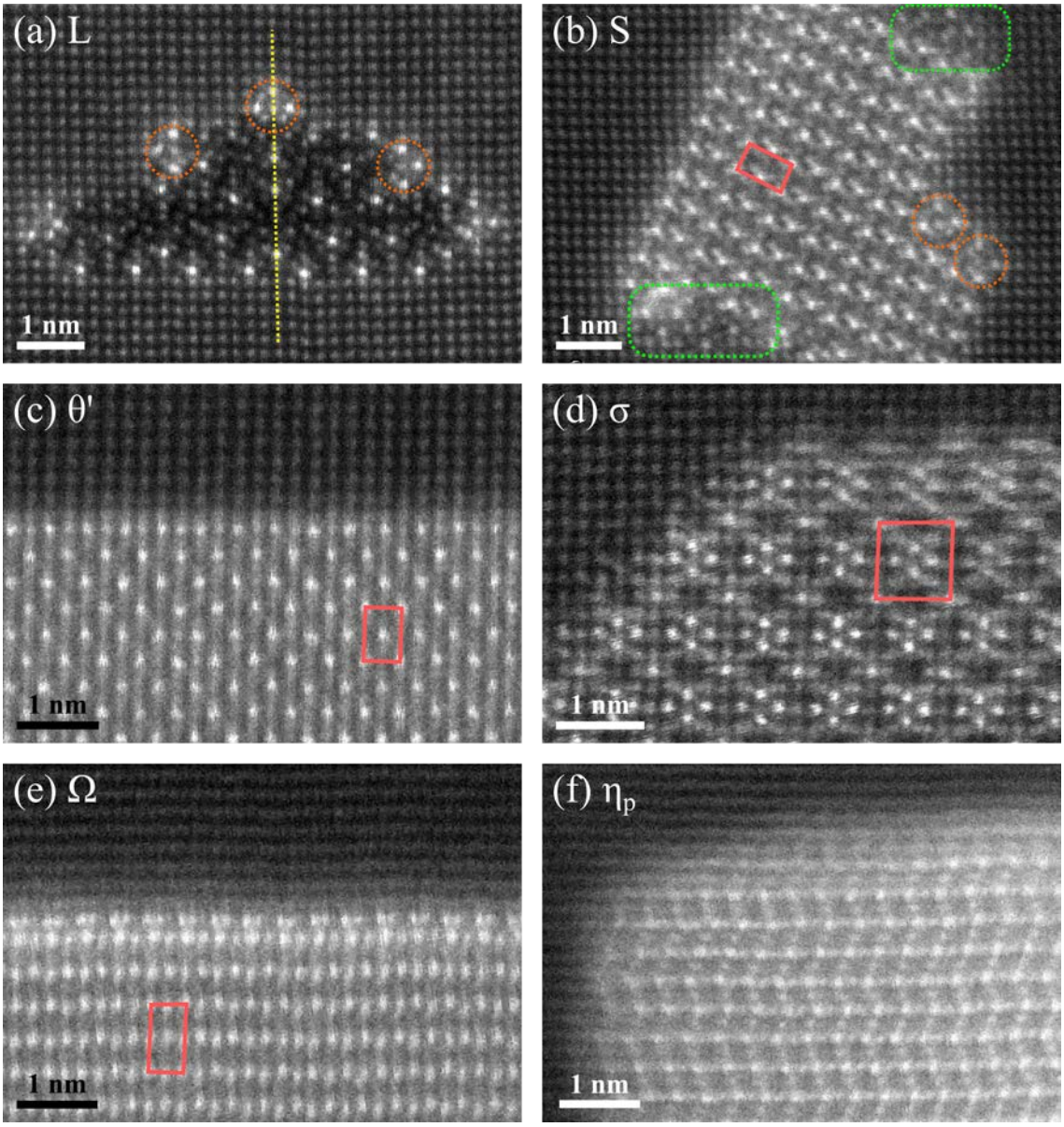

Fig. 2.

The needle-shaped particles from the peak aged condition grow thicker and longer during the over-ageing. The structures are diverse, but they will be colloquially referred to as L, which is descriptive of most observed particles. L is a disordered phase, meaning that it has no unit cell repeating in its cross-sectional plane [30], although it contains structural elements from the C and Q' phases, as well as phases from the Al–Mg–Si system hosting a Si network [28]. Many of the particles are connected to GPB-zone units from the Al–Cu–Mg system [31], as marked

with dotted circles in Fig. 2(a). In spite of structural disorder, many particles of the L type exhibit other global symmetries such as two-fold rotation and mirror planes (partial mirror plane marked with a dotted line). Similar symmetries have been spotted in Al–Mg–Si–Ge–Cu alloys [32].

S–Al_2CuMg [33,34,35] is found less frequently than L. GPB units, which usually play the role of nucleating the S phase [11], are commonly observed on the S–Al interfaces. The same are Si-containing disordered regions typical of L phases, marked with rounded rectangles on Fig. 2(b).

The most apparent features in Fig. 1(b) are bright streaks which turn out to be θ'–Al_2Cu [36] plates on $\{100\}_{Al}$ planes. They appear to occupy the highest volume fraction of all precipitate phases, and thus claim the highest amount of Cu. Cubic σ–$Al_5Cu_6Mg_2$ [37] particles are also present. They were observed in great numbers in alloys similar to ours excluding Zn, aged at high temperatures [38].

A few Ω–Al_2Cu [39,40] is formed as thick plates on $\{111\}_{Al}$ planes. It can form with two distinct orientation relationships to the Al matrix: $[112]_{Al} \parallel [001]_{\Omega}$ and $[112]_{Al} \parallel [011]_{\Omega}$ (as in Fig. 2(e)). The composition of the enriched Ω–Al interface is discussed in section 3.3.

Despite the high Zn content in the alloy, the least common phase in the over-aged condition is η_p [20] (Type 2 from [19]). Most of the Zn must therefore remain in solid solution, which is reasonable due to its high solubility in Al. Some Zn was also measured in most Cu-containing phases, where it may partially occupy Cu sites due to the similar bonding nature of these elements. Similarly, Cu can replace Zn in η-type precipitates [41,42], and Zn can occupy some typical Cu sites in Al–Mg–Si(–Cu) precipitates [43].

3.2. Nucleation

Though most particles adhere to one of the former classifications, many complexes of several phases were also observed, the most interesting of which appears to have been recently heterogeneously nucleated. Two such cases were seen on neighboring L precipitates in Fig. 3(a), one showing clear σ unit cells and the other resembling a θ' nucleus. Due to the strong intensity of the Cu columns, and the apparent lack of precipitate–matrix overlap, both nuclei must be needle-like. The growth rate of these phases should be limited primarily by the available Cu, which is required by all phases present. A layer of C phase is present at the right side of the θ' nucleus, which is discussed in section 3.4. Fig. 3(b) shows a complex of an S phase and a disordered Al–Mg–Si–Cu phase. Since only the latter is observed in the peak hardness condition, it most likely constituted the original precipitate, and an S nucleus formed on or inside it, eventually growing to split it into two parts. On a side note, the hexagonal section in the lower part is isostructural to β'–Ag [44,45], with either Cu or Zn playing the role of Ag. Another complex of intergrown phases is presented in Fig. 4. Plates of Ω and η_p (identified by lattice imaging) are viewed edge-on, with two other rounded plates on either $\{100\}_{Al}$ or $\{111\}_{Al}$ planes connecting to the middle part. With Ω and θ' typically having well-defined faceted edges [46,47], the plates are most likely to be an η-type phase.

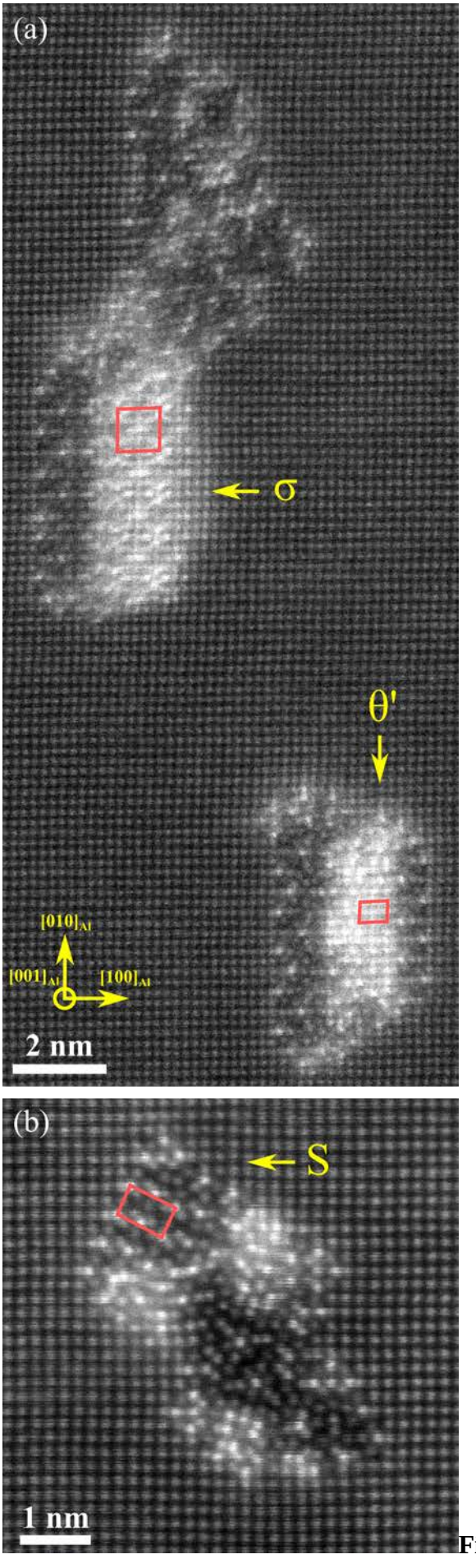

Fig. 3.

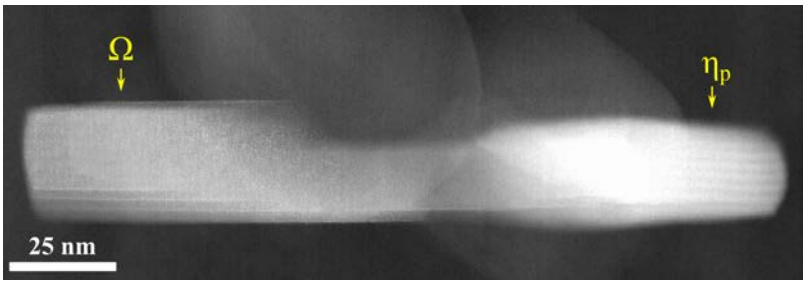

Fig. 4.

Only the first of the phases presented in Fig. 2 contains Si. Nonetheless, the diversity of phases is attributed to the Si content of the alloy. Fig. 3 provides a hint to why: The initial, Si-containing needles along $<001>_{Al}$ provide excellent nucleation points for other phases with $<001>_{Al}$ coherencies, namely S, θ' and σ, while the plates on $\{111\}_{Al}$ planes, Ω and η_p, are suppressed. On removing Si from the composition, the needles would not have appeared, leaving η-type phases as the most favorable to nucleate and ensuring a dominance of $<111>_{Al}$ coherency through the entire aging process [48].

3.3. Ω and its Interface with Al

Though the bulk of the Ω phase has composition Al_2Cu, it is predominantly observed with both Ag and Mg in its interface layer [38], which is a $\{111\}_{Al}$ plane with Al substituted with the stoichiometry Ag_2Mg. In rare cases it can also precipitate without the aid of Ag [49]. To investigate the composition of the interface layers of Ω in our alloy, we conducted EDS mapping with near-atomic resolution of an Ω plate. The measurements are presented in Fig. 5. The results are unambiguous: the elements Zn and Mg have strong signals at the Ω–Al interface, and no significant counts elsewhere. A replacement of Ag with Zn is plausible, as the interface sites are very similar to fcc-Al sites, which both elements like occupying, due to their excellent solubility in Al [50]. Fig. 5(f) shows the atomic model adapted from Kang et al.

[38] with our elemental replacement. The interface layer is identical to the proposed layer between plate-shaped GP–η_p/ η_p particles and Al [19].

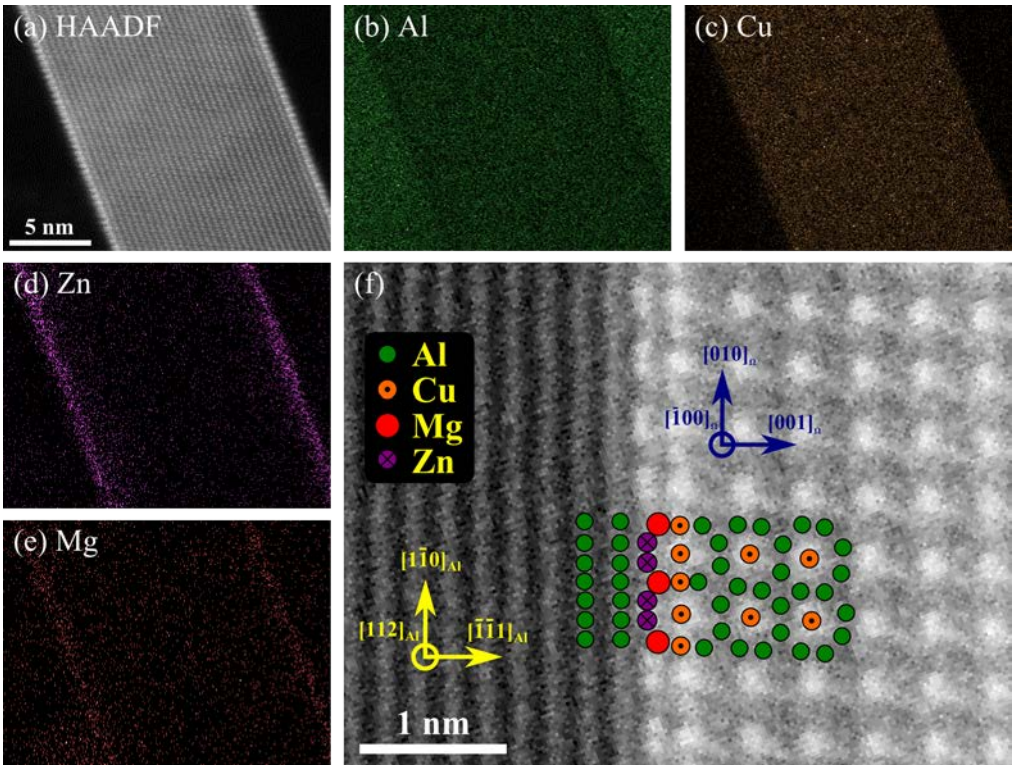

Fig. 5.

3.4. θ'–C Plates

Continuing the discussion on cross-system nucleation, we dive into the case of θ' plates interacting with other phases. By observation, such occurrences can be divided into two classes. The first one is disordered L-like particles on semi-coherent edges or on $\{100\}_{Al}$ ledges of θ' plates. Similar complexes were found in an alloy with a higher Cu/Mg ratio [51]. Additionally, θ'–S complexes were found in a similar alloy without Si [52]. The second class, which will be given focus, is one layer of C phase on the coherent θ'–Al interface. Two such layers would constitute a full C plate [17]. The θ'–C plates, one of which is shown in Fig. 6, are structurally ordered and consistent. The shown θ' unit cell adapts the well-established Silcock structure [34]. Otherwise, the proposed atomic model is created based on how the

structures might best fit together. The interface layer between θ’ and Al keeps the fcc-Al structure but with full Cu occupation [47]. However, the corresponding layer interfaced with C is more reminiscent to the bulk θ’ Cu layers. Outside this layer, the θ’ phase wants another layer of Al while the C phase wants a layer with every other Mg and Si column. These two interface layers, which may contain a mix of elements, is marked with dashed lines in Fig. 6. Looking at the Cu columns, every other θ’ column is present across the interface, as shown with unbroken lines. This makes these two plate-shaped phases quite compatible. The adhesion of a C layer to a θ’ precipitate is interesting as it affects the strain surrounding its coherent interfaces, in addition to helping the nucleation and growth of the phase.

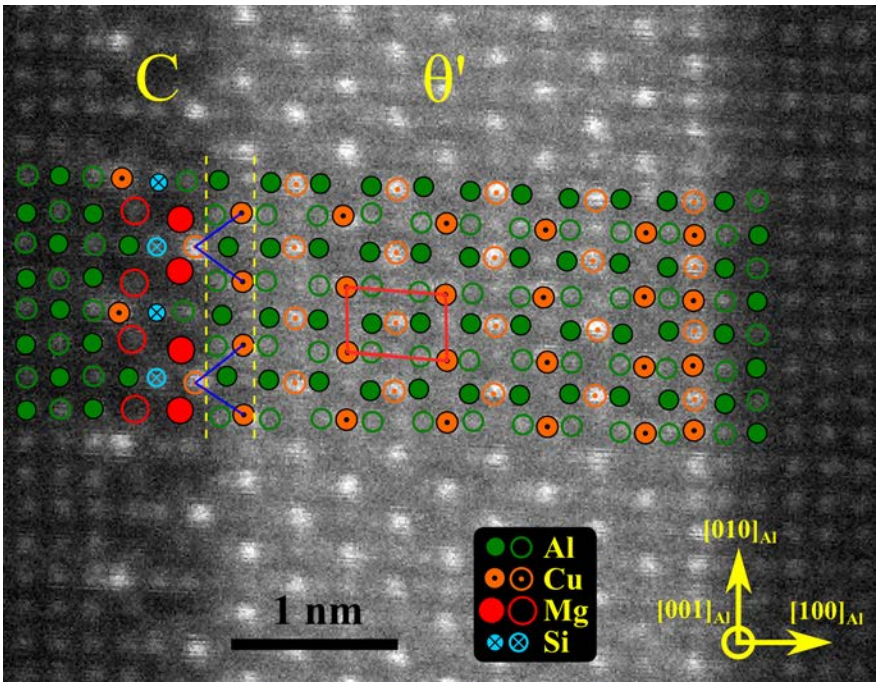

Fig. 6.

4. Conclusion

An aluminium alloy containing Zn, Cu, Mg and Si was investigated. The microstructure in the alloy is dominated by Si-containing disordered needle-shaped precipitates along <001>$_{Al}$ from

the solid solution stage through peak hardness, while prolonged aging produces a variety of phases associated with the systems Al–Cu, Al–Cu–Mg, Al–Mg–Si–Cu and Al–Zn–Mg and even Al–Cu–Mg–Ag. The phases S, θ' and σ, which have one or more directions coherent with $<001>_{Al}$, were shown through direct observation to be nucleated on the existing needles, often co-growing with them. In addition, Ω and η_p phases formed during the over-aging. Two previously unseen cases of special interest that transcend several alloy systems were found: Ω plates with Ag replaced by Zn on its interface with Al, and θ' plates with one layer of C phase on their coherent interfaces. The study has revealed the nucleation behavior of various phases and has shed light on the relationships between different alloy systems and how their microstructures may be merged.

Acknowledgements
The authors would like to thank the Research Council of Norway for funding of the FRINATEK project "Fundamental investigations of precipitation in the solid state with focus on Al-based alloys".

[1] R. H. Jones, V. F. Zackay, E. R. Parker, “Laves phase precipitation in Fe-Ta alloys”, *Metall. Trans.*, **1972**, *3*, 2835.

[2] Z. Zhang, C. T. Liu, M. K. Miller, X.-L. Wang, Y. Wen, T. Fujita, A. Hirata, M. Chen, G. Chen, B. A. Chin, “A nanoscale co-precipitation approach for property enhancement of Fe-base alloys”, *Sci. Rep.*, **2013**, *3*, 1327.

[3] M. Takeda, K. Inukai, N. Suzuki, G. Shinohara, H. Hashimoto, “Precipitation behaviour of Cu–Co alloys”, *Phys. Stat. Sol.* **1996**, *158*, 39.

[4] S. A. Lockyer, F. W. Noble, “Precipitate structure in a Cu-Ni-Si alloy”, *J. Mater. Sci.*, **1994**, *29*, 218.

[5] M. Nishijima, K. Hiraga, “Structural Changes of Precipitates in an Mg-5 at%Gd Alloy Studied by Transmission Electron Microscopy”, *Mater. Trans.*, **2007**, *48*, 10.

[6] Y. Matsuoka, K. Matsuda, K. Watanabe, J. Nakamura, W. Lefebvre, D. Nakagawa, S. Saikawa, S. Ikeno, “Precipitation Sequence in the Mg-Gd-Y System Investigated by HRTEM and HAADF-STEM”, *Mater. Trans.*, **2014**, *55*, 1051.

[7] I MacLaren1, L. Q. Wang, B. Schaffer, Q. M. Ramasse, A. J. Craven, S. M. Selbach, N. A. Spaldin, S. Miao, K. Kalantari, I. M. Reaney, “Novel Nanorod Precipitate Formation in Neodymium and Titanium Codoped Bismuth Ferrite”, *Adv. Funct. Mater.*, **2012**, *23*, 683.

[8] A. Wilm, “Physikalisch-metallurgische Untersuchungen über magnesiumhaltige Aluminiumlegierungen”, *Metallurgie* **1911**, *8*, 225.

[9] P. D. Merica, R. G. Waltenberg, H. Scott, “Heat treatment of duralumin”, *Sci. Pap. Bur. Stand.* **1919**, *15*, 271.

[10] S. P. Ringer, K. Hono, “Microstructural Evolution and Age Hardening in Aluminium Alloys: Atom Probe Field-Ion Microscopy and Transmission Electron Microscopy Studies”, *Mater. Charact.*, **2000**, *44*, 101.

[11] S. C. Wang, M. J. Starink, “Precipitates and intermetallic phases in precipitation hardening Al–Cu–Mg–(Li) based alloys”, *Int. Mater. Rev.*, **2005**, *50*, 193.

[12] C. D. Marioara, S. J. Andersen, H. W. Zandbergen, R. Holmestad, “The Influence of Alloy Composition on Precipitates of the Al-Mg-Si System”, *Metall. Mater. Trans. A*, **2005**, *36A*, 691.

[13] C. R. Hutchinson, S. P. Ringer, “Precipitation Processes in Al-Cu-Mg Alloys Microalloyed with Si”, *Metall. Mater. Trans. A* **2000**, *31*, 2721.

[14] H. W. Zandbergen, S. J. Andersen, J. Jansen, “Structure Determination of Mg_5Si_6 Particles in Al by Dynamic Electron Diffraction Studies”, *Science* **1997**, *277*, 1221.

[15] D. J. Chakrabarti, D. E. Laughlin, “Phase relations and precipitation in Al–Mg–Si alloys with Cu additions”, *Prog. Mater. Sci.*, **2004**, *49*, 389.

[16] C. Cayron, L. Sagalowicz, O. Beffort, P. A. Buffat, “Structural phase transition in Al-Cu-Mg-Si alloys by transmission electron microscopy study on an Al-4 wt% Cu-1 wt% Mg-Ag alloy reinforced by SiC particles”, *Philos. Mag. A*, **1999**, 79, 2833.

[17] M. Torsæter, F. J. H. Ehlers, C. D. Marioara, S. J. Andersen, R. Holmestad, “Applying precipitate–host lattice coherency for compositional determination of precipitates in Al–Mg–Si–Cu alloys”, *Phil. Mag.*, **2012**, *92*, 3833.

[18] Y.-Y. Li, L. Kovarik, P. J. Philips, Y.-F. Hsu, W.-H. Wang, M. J. Mills, “Ab initio analysis of Guinier–Preston–Bagaryatsky zone nucleation in Al–Cu–Mg alloys”, *Phil. Mag. Lett.*, **2012**, *92*, 166.

[19] C. D. Marioara, W. Lefebvre, S. J. Andersen, J. Friis, “Atomic structure of hardening precipitates in an Al–Mg–Zn–Cu alloy determined by HAADF-STEM and first-principles calculations: relation to η-$MgZn_2$”, *J. Mater. Sci.*, **2013**, *48*, 3638.

[20] J. Z. Liu, J. H. Chen, Z. R. Liu, C. L. Wu, “Fine precipitation scenarios of AlZnMg(Cu) alloys revealed by advanced atomic-resolution electron microscopy study Part I: Structure determination of the precipitates in AlZnMg(Cu) alloys”, *Mater. Char.*, **2015**, *99*, 277.

[21] S. J. Pennycook, D. E. Jesson, A. J. McGibbon, P. D. Nellist, “High Angle Dark Field STEM for Advanced Materials”, *J. Electron Microsc.*, **1996**, *45*, 36.

[22] A. V. Crewe, J. Wall, J. Langmore, “Visibility of Single Atoms”, *Science*, **1970**, *168*, 1338.

[23] M. Isaacson, D. Kopf, M. Utlaut, N. W. Parker, A. V. Crewe, “Direct observations of atomic diffusion by scanning transmission electron microscopy”, *Proc. Natl. Acad. Sci. USA*, **1977**, *74*, 1802.

[24] S. J. Pennycook, M. Varela, A. R. Lupini, M. P. Oxley, M. F. Chrisholm, “Atomic-resolution spectroscopic imaging: past, present and future”, *J. Electron Microsc.*, **2009**, *58*, 87.

[25] G. Kothleitner, M. J. Neish, N. R. Lugg, S. D. Findlay, W. Grogger, F. Hofer, L. J. Allen, “Quantitative Elemental Mapping at Atomic Resolution Using X-Ray Spectroscopy”, *Phys. Rev. Lett.*, **2014**, *112*, 085501.

[26] Y. J. Li, L. Arnberg, “Quantitative study on the precipitation behavior of dispersoids in DC-cast AA3003 alloy during heating and homogenization”, *Acta Mater.*, **2003**, *51*, 3415.

[27] Z. Q. Feng, Y. Q. Yang, B. Huang, M. H. Li, Y. X. Chen, J. G. Ru, “Crystal substructures of the rotation-twinned T ($Al_{20}Cu_2Mn_3$) phase in 2024 aluminum alloy”, *J. Alloy. Compd.* **2014**, *583*, 445.

[28] F. J. H. Ehlers, S. Wenner, S. J. Andersen, C. D. Marioara, W. Lefebvre, C. B. Boothroyd, R. Holmestad, “Phase stabilization principle and precipitate-host lattice influences for Al–Mg–Si–Cu alloy precipitates”, *J. Mater. Sci.* **2014**, *49*, 6413.

[29] S. J. Andersen, C. D. Marioara, R. Vissers, A. Frøseth, H. W. Zandbergen, “The structural relation between precipitates in Al–Mg–Si alloys, the Al-matrix and diamond silicon, with emphasis on the trigonal phase U1-$MgAl_2Si_2$”, *Mater. Sci. Eng. A*, **2007**, *444*, 157.

[30] C. D. Marioara, S. J. Andersen, T. N. Stene, H. Hasting, J. Walmsley, A. T. J. van Helvoort, R. Holmestad, “The effect of Cu on precipitation in Al–Mg–Si alloys”, *Phil. Mag.* **2007**, *87*, 3385.

[31] L. Kovarik, S. A. Court, H. L. Fraser, M. J. Mills, “GPB zones and composite GPB/GPBII zones in Al–Cu–Mg alloys”, *Acta Mater.*, **2008**, *56*, 4804.

[32] R. Bjørge, S. J. Andersen, C. D. Marioara, J. Etheridge, R. Holmestad, “Scanning transmission electron microscopy investigation of an Al–Mg–Si–Ge–Cu alloy”, *Phil. Mag.*, **2012**, *92*, 3983.

[33] Z. R. Liu, J. H. Chen, S. B. Wang, D. W. Yuan, M. J. Yin, C. L. Wu, “The structure and the properties of S-phase in AlCuMg alloys”, *Acta Mater.* **2011**, *59*, 7396.

[34] S. B. Wang, J. H. Chen, M. J. Yin, Z. R. Liu, D. W. Yuan, J. Z. Liu, C. H. Liu, C. L. Wu, “Double-atomic-wall-based dynamic precipitates of the early-stage S-phase in AlCuMg alloys”, *Acta Mater.* **2012**, *60*, 6573.

[35] H. Perlitz, A. Westgren, “The Crystal Structure of Al2CuMg“, *Ark. Kemi. Mineral Geol.*, **1943**, *16B*, 1.

[36] J. M. Silcock, T. J. Heal, H. K. Hardy, “Structural Ageing Characteristics of Binary Aluminium-Copper Alloys”, *J. Inst. Met.,* **1953**, *82*, 239.

[37] S. Samson, “Die Kristallstruktur von $Mg_2Cu_6Al_5$”, *Acta Chem. Scand.* **1949**, *3*, 809.

[38] S. C. Barr, L. M. Rylands, H. Jones, W. M. Rainforth, “Formation and characteristics of coarsening resistant cubic sigma phase in AI-4.2Cu-1.6Mg-0.2Si.”, *Mater. Sci. Tech.*, **1997**, *13*, 655.

[39] Y. C. Chang, J. M. Howe, “Composition and Stability of Ω Phase in an Al-Cu-Mg-Ag Alloy”, *Metal. Trans. A*, **1993**, *24*, 1461.

[40] S. J. Kang, Y.-W. Kim, M. Kim, J.-M. Zuo, “Determination of interfacial atomic structure, misfits and energetics of Ω phase in Al–Cu–Mg–Ag alloy”, *Acta Mater*. **2014**, *81*, 501.

[41] T. Marlaud, A. Deschamps, F. Bley, W. Lefebvre, B. Baroux, “Influence of alloy composition and heat treatment on precipitate composition in Al–Zn–Mg–Cu alloys”, *Acta Mater.*, **2010**, *58*, 248.

[42] S. Wenner, C. D. Marioara, W. Lefebvre, Q. M. Ramasse, D.-M. Kepaptsoglou, F. S. Hage, R. Holmestad, "Atomic-resolution elemental mapping of precipitates in a 7449 aluminium alloy", *Mater. Sci. Forum*, **2014**, *794–796*, 63.

[43] T. Saito, S. Wenner, E. Osmundsen, C. D. Marioara, S. J. Andersen, J. Røyset, W. Lefebvre, R. Holmestad, "The effect of Zn on precipitation in Al–Mg–Si alloys", *Phil. Mag.*, **2014**, *94*, 2410.

[44] J. Nakamura, K. Matsuda, T. Kawabata, T. Sato, Y. Nakamura, "Effect of Silver Addition on the β'-Phase in Al-Mg-Si-Ag Alloy", S. Ikeno, *Mater. Trans.*, **2010**, *51*, 310.

[45] C. D. Marioara, J. Nakamura, K. Matsuda, S. J. Andersen, R. Holmestad, T. Sato, T. Kawabata, S. Ikeno, "HAADF-STEM study of β'-type precipitates in an over-aged Al–Mg–Si–Ag alloy", *Phil. Mag.*, **2012**, *92*, 1149.

[46] B. C. Muddle, I. J. Polmear, "The precipitate Ω phase in Al-Cu-Mg-Ag alloys", *Acta. metall.*, **1989**, *37*, 777.

[47] L. Bourgeois, N. V. Medhekar, A. E. Smith, M. Weyland, J.-F. Nie, C. Dwyer, "Efficient Atomic-Scale Kinetics through a Complex Heterophase Interface", *Phys. Rev. Lett.* **2013**, *111*, 046102.

[48] S. Wenner, unpublished results.

[49] A. Garg, Y. C. Chang, J. M. Howe, "Precipitation of the Ω Phase in an Al-4.0Cu-0.5Mg Alloy", *Scripta Metall. Mater.* **1990**, *24*, 677.

[50] J. R. Davis, editor, *Aluminium and Aluminium Alloys*, 46 Speciality handbook, 46 International, **1993**.

[51] L. Liu, J. H. Chen, S. B. Wang, C. H. Liu, S. S. Yang, C. L. Wu, "The effect of Si on precipitation in Al–Cu–Mg alloy with a high Cu/Mg ratio", *Mater, Sci. Eng. A* **2014**, *606*, 187.

[52] J. Z. Liu, S. S. Yang, S. B. Wang, J. H. Chen, C. L. Wu, "The influence of Cu/Mg atomic ratios on precipitation scenarios and mechanical properties of Al–Cu–Mg alloys", *J. Alloy. Compd.* **2014**, *613*, 139.

Fig. 1. Precipitate microstructure. (a) Overview bright-field TEM image of the peak-aged condition, 150 °C for 17 hours. (b) HAADF–STEM image of the precipitate microstructure in a very over-aged condition, 150 °C for 32 days. (c–d) HAADF–STEM images of the peak-aged condition, showing example cross-sections of needle-shaped particles. Somewhat distorted Si networks are marked with yellow lines. (e–j) STEM–EDS map of a group of precipitates in the peak-aged condition, showing the presence of Mg, Si, Zn and Cu.

Fig. 2. The 6 phases observed in the over-aged condition, 150 °C for 32 days. HAADF–STEM images acquired along direction $<001>_{Al}$ in (a–d), and $<112>_{Al}$ (with horizontal $\{111\}_{Al}$ planes) in (e–f). An unbroken line signifies a unit cell where applicable. In (a–b), the orange dotted circles mark the location of GPB structural units. The vertical dotted yellow line in (a) show the presence of a local mirror symmetry, while the green dotted lines in (b) mark Si-containing disordered areas.

Fig. 3. Phases nucleating from needle-shaped precipitates similar to the one in Fig. 2(a). Images are in the over-aged condition (150 °C for 32 days), and both are viewed along the $<001>_{Al}$ direction. An unbroken line signifies a unit cell where applicable. (a) Nucleation of σ and θ’ phases. (b) Nucleation of an S phase.

Fig. 4. Intergrown Ω and η_p particles on horizontal $\{111\}_{Al}$ planes. Plate-shaped particles growing on different Al planes connect to the middle part. Observed in the $<112>_{Al}$ direction.

Fig. 5. Composition determination of the interfacial layer between the Ω phase and the Al matrix. (a) HAADF–STEM image of an Ω precipitate, viewed along the $[112]_{Al} \parallel [001]_{\Omega}$ direction. (b–e) Energy dispersive X-ray spectroscopy (EDS) maps of the same region. The lines in the Zn and Mg maps overlap exactly with the bright interfacial layer. (f) The proposed atomic structure of the Ω phase [38], (2D projection) with Ag replaced by Zn, as an overlay on a high-resolution STEM image.

Fig. 6. One example of a combined θ’–C plate. The atomic overlay is made from the accepted structures of the two phases, although some mixed atomic columns might occur. Filled and non-filled circles denote distinct half-layers, approximately 203 pm apart in the $[001]_{Al}$ direction.